Cellular and Molecular Biology
E-ISSN : 1165-158X / P-ISSN : 0145-5680
www.cellmolbiol.org

Estrogens desensitize MCF-7 breast cancer cells to apelin-induced autophagy and enhanced growth under estrogen starvation: a possible implication in endocrine resistance

Rim Bouchelaghem[1], Sylvie Mader[2,3], Louis Gaboury[2,3], Mahfoud Messarah[1], Mahieddine Boumendjel[1], Amel Boumendjel[1*]

[1] Laboratoire de Biochimie et Toxicologie Environnementale, Département de Biochimie, Faculté des Sciences, Université Badji Mokhtar, Annaba, Algérie
[2] Institute for Research in Immunology and Cancer, University of Montreal, Montreal, QC, Canada
[3] Department of Biochemistry, Faculty of Medicine, University of Montreal, Montreal, QC, Canada

ARTICLE INFO

Original paper

Article history:
Received: July 29, 2022
Accepted:September 14, 2022
Published: September 30, 2022

Keywords:

Apelin-13, MCF-7, breast cancer, estrogen starvation, endocrine resistance.

ABSTRACT

Apelin-13 is an adipokine known for its growth-inducing effects on human breast cancer cells in an estrogen-containing environment. However, the response of these cells to apelin-13 in the absence of estrogen and its association with the expression of the apelin receptor (APLNR) has not yet been investigated. In the present study, we show that the breast cancer cell line MCF-7 expresses the APLNR as shown by immunofluorescence and flow cytometry, under conditions of ER starvation and that culture of these cells in the presence of apelin-13 results in an increased growth rate and a diminished autophagy flux. Moreover, the binding of APLNR by apelin-13 resulted in an increased growth rate (assayed by AlamarBlue) and a diminished autophagy flux (monitored by Lysotracker Green). The latter observations were reversed in the presence of exogenous estrogen. Finally, apelin-13 induces the deactivation of the apoptotic kinase AMPK. Taken together, our results show that APLNR signaling in breast cancer cells is functional and prevents tumor growth under conditions of estrogen starvation. They furthermore suggest an alternative mechanism of estrogen-independent tumor growth thereby positioning the APLNR-AMPK axis as a novel pathway and a possible therapeutic target in endocrine resistance of breast cancer cells.

Doi: http://dx.doi.org/10.14715/cmb/2022.68.9.18

Introduction

Estrogen receptor-expressing (ER^+) breast carcinoma cells require estrogen-driven signals to proliferate. Endocrine therapy is based on different approaches that aim at suppressing cancer growth (1, 2). Therapeutic approaches consist either in the inhibition of estradiol responsiveness by blocking or downregulating its receptor or the reduction of estradiol concentration in serum and mammary tissue. However, the efficacy of endocrine therapy is limited by the ability of human breast cancer cells to circumvent the resulting growth inhibition. The consequence is the emergence of tumor cells that grow even under estrogen starvation, resulting in treatment-resistant, and often incurable, diseases. Subsequently, ER+ tumor cells, which are initially dependent on estrogen for their proliferation, continue to respond to different proliferation-stimulating factors by growing at a heightened rate (3).

In laboratory models of ER^+ breast cancer, growth adaptation to estrogen starvation can be induced by growing cells in a conditioned culture medium depleted of estrogen. The Michigan Cancer Foundation-7 (MCF-7) cell line, derived from a human breast adenocarcinoma, is the most extensively used experimental tool to study ER^+ tumor endocrine resistance *in vitro* (4, 5). Indeed, long-term estrogen starvation of MCF-7 cells eventually promotes proliferation via estrogen-independent mechanisms, such as those under the control of the adipokines leptin (6), adiponectin (7, 8) or resistin (9). Interestingly, a common regulatory mechanism of leptin and adiponectin-mediated growth of MCF-7 cells is autophagy (10, 11) , an intracellular process leading to the degradation of damaged or dysfunctional subcellular organelles (12). Accumulating evidence has shown that autophagy plays a prominent role in sustaining breast cancer cell survival rather than promoting cell death in the case of established tumors (13). Indeed, autophagy has been linked to the restoration of endocrine sensitivity and the promotion of breast cell growth (14).

Apelin, another adipokine, is known for its regulatory growth in an autophagy-dependent manner in cardiovascular and neurodegenerative diseases (15, 16). However, apelin-induced autophagy as a mechanism in promoting cancer cell growth remains poorly investigated and has been studied only in the four human cell models, the lung adenocarcinoma (17), the colon adenocarcinoma (18), the cholangiocarcinoma (19) and the hepatoma cell model Hepatoma G2 (HepG2) (20). It will be of interest to examine whether the well-established role of apelin in regulating autophagy in reoxygenation is operational in breast cancer disease as well.

Consistent with this hypothesis, it has been demonstrated that apelin mediates a proliferative effect under estrogen starvation in $ER\alpha^+$ MCF-7 cells (21). In addition,

* Corresponding author. Email: amelibis@yahoo.fr; amel.boumendjel@univ-annaba.org

several studies have shown a positive association between circulating apelin levels and the risk of developing endocrine therapy resistance (22). It will therefore be interesting to address whether apelin regulates MCF-7 cell growth in an autophagy-dependent manner in the absence of estrogen.

In the present study, we have addressed the expression of APLNR in the MCF-7 cell line and compared the role of apelin-13 in their proliferation in short-term culture under estrogen starvation or in the presence of E2. We have also investigated whether APLNR activation by apelin promotes the autophagy of MCF-7 and affected the Adenosine monophosphate-activated protein kinase (AMPK)-autophagy pathway.

Materials and Methods

Antibodies and reagents

Antibodies raised against apelin receptor (APLNR) (sc-517300, mouse) were from Santa Cruz Biotechnology (Dallas, Texas, USA); antibodies against total AMPKα (2532, rabbit), phospho-AMPKα (Thr^{172}) (2535, rabbit) were obtained from Cell Signaling Technology (Beverly, MA, USA); antibody raised against fluorescein isothiocyanate (FITC) conjugated-α-Tubulin (F2168, rabbit) was purchased from Sigma-Aldrich (St. Louis, Missouri, USA). Horseradish peroxidase (HRP)-conjugated secondary antibodies (111-035-003, rabbit) and (115-035-003, mouse) were purchased from Cedarlane (Burlington, Canada). 17β-estradiol (E2; E2758) was purchased from Sigma-Aldrich (St. Louis, Missouri, USA). Apelin-13 (13523) was obtained from Cayman Chemical, (Michigan, USA). Lowry assay was obtained from Bio-Rad (Hercules, CA). Western Blot Chemiluminescence Reagent Plus system was obtained from (NEN Life Science Products). AlamarBlue assay was purchased from Invitrogen (Indianapolis, USA). The Lysotracker green (L7526) was purchased from Thermofisher (San Diego, California, USA).

Cell culture

MCF-7 human breast adenocarcinoma cell line and HEK293 Cell line were purchased from the American Type Culture Collection (ATCC) (Manassas, VA, USA) and were regularly tested for mycoplasma contamination. MCF-7 cells were maintained in Dulbecco's modified eagle medium (DMEM) (Wisent 310–005 (St-Bruno, Québec, Canada)) supplemented with 10% (v/v) fetal bovine serum (FBS) (FBS, Sigma-Aldrich, F1051, Ontario, Canada), 1% L-glutamine (Wisent 609–065), and 1% penicillin-streptomycin (Wisent 450–201). Three days before experiments, MCF-7 cells were switched to phenol red-free DMEM (Wisent 319–050) containing charcoal-stripped FBS, 2% L-glutamine, and 1% penicillin-streptomycin. Three days before experiments, cells were harvested and cultured under starvation in an estrogen-deprived medium, composed from the phenol red-free Alpha MEM (Wisent 310–011 (St-Bruno, Québec, Canada)) supplemented with 10% dextran-coated charcoal-stripped FBS, 2% L-glutamine, 1% penicillin-streptomycin in different dishes as mentioned in each experiment. MCF-7 and HEK293 cell lines were washed with Phosphate-Buffered Saline (PBS) and then trypsinized until detachment from the bottom of the dish, then media specific for each cell line was added to inactivate trypsin. Cells and media were collected in a 15 mL tube and centrifuged at 1000 rotations per minute (rpm) for 5 minutes. Cells were trypsinized by adding 2 mL of trypsin solution to 15-cm Petri dishes followed by 3 min incubation at 37°C with regular gentle shaking. The trypsin reaction was stopped by adding 6 mL of phenol-free culture medium containing 10% FCS charcoal. The number of cells in the suspension was then counted with a Fuchs–Rosenthal hemocytometer and brought first to a concentration of 1×10^6 cells/mL Cells were seeded in 6 well culture dishes at the density 1×10^6 cells, and after reaching log phase, cells were trypsinized as mentioned above. The supernatant was dropped, and the cell pellets were processed as mentioned in each experiment. HEK-293 cells were maintained in DMEM supplemented with 10% FBS and 1% penicillin-streptomycin growing medium in 15-cm Petri dishes culture in a humidified 5% CO_2 atmosphere at 37°C until they reached 80% confluence.

Preparation of Formalin-Fixed Paraffin-Embedded cell pellets

MCF-7 cells were maintained under estrogen starvation in the growing medium in 15-cm Petri dishes culture in a humidified 5% CO_2 atmosphere at 37°C until they reached 80% confluence. MCF-7 and HEK293 cell lines were washed with PBS and then trypsinized until detachment from the bottom of the dish, then media specific for each cell line was added to inactivate trypsin. Cells and media were collected in a 15 mL tube and centrifuged at 1000 rotations per minute (rpm) for 5 minutes. The supernatant was dropped, and the cell pellets were immediately used to prepare Formalin-fixed paraffin-embedded (FFPE) cell blocks. Briefly, the pellet cells were resuspended in 10% neutral buffered formalin at room temperature for one hour to allow proper fixation. The cells were centrifuged at 2000 rpm for 10 minutes, and the supernatant was discarded. Richard-Allan Scientific HistoGel Specimen Processing Gel (22-110-678, Fisher Scientific) was heated at 60°C and converted to a liquid state which is maintained at 50°C, and four to five drops of melted HistoGel were then added and mixed to each pellet. The mixture was placed at room temperature and allowed to solidify. The HistoGel was then removed from the Eppendorf tubes and placed in embedding cassettes for further fixation in 10% buffered formalin for one hour at room temperature. The cell blocks included in a cassette were next processed in SAKURA Tissue-Tek VIP (Vacuum infiltration processor) and recirculated according to the standard paraffin infiltration schedule. Briefly, the first step of circulation consists of getting paraffin into the cells. Next, the cells were dehydrated in three alcohol baths with increasing concentrations at 70%, 85% and 90% to altogether remove the water from the cells. Three successive baths of 100% toluene realized the lightning. Cells were then embedded in hot paraffin baths (44˚C to 60˚C) and 4 µm section from each block was prepared for further analysis.

Preparation of Formalin-Fixed Paraffin-Embedded tissue

FFPE of positive and negative control tissues were prepared as follows. For this, tissue is fixed in 10% neutral buffered formalin (Bios Europe, Lancashire, UK) overnight at room temperature, then processed using a Tissue-Tek VIP automatic tissue processor (Sakura, Finland) with a standard 14 hours protocol and embedded into paraf-

fin wax (Tissue-Tek). 3–4 µm sections were cut from the embedded blocks and floated onto a warm (42°C) water bath from where they were picked up onto Superfrost plus slides (Cat No 631–0108, VWR International, Lutterworth, Leicestershire, UK). Slides were placed in a vertical rack and dried overnight at 37°C in a fan-assisted cabinet. The next day, slides were dated and placed in a container which was then purged with oxygen-free nitrogen gas (BOC gases, Guildford, Surrey, UK). The containers were stored at 4°C. To carry out a labelling experiment, the required slides were removed and the container with the remaining slides was again purged with oxygen-free nitrogen gas before replacing at 4°C. Briefly, FFPE sections of MCF-7, HEK293 cells, ER^+ breast carcinoma, stomach and muscle tissues were cut into 4 µm sections with a microtome (Micom) and were subsequently transferred to charged slides.

Automated immunohistochemistry

Automated IHC was carried out according to manufacturer recommendations on an automated immunostainer Leica Bond RX (Leica, Concord, Ontario, Canada). The Leica Intense R DS9263 kit was applied according to proprietary guidelines. Briefly, the sections of MCF-7 or HEK293 cells were deparaffinized followed by an Antigen retrieval and was performed at 100 ° C for 20 minutes. Then the APLNR antibody was applied at 1/100 dilution, at room temperature, for 30 minutes. A secondary anti-mouse antibody coupled to biotin and diluted to 1/100 (Jackson ImmunoResearch) was then applied to sections for 15 minutes at room temperature.

The Ag-Ac reaction was revealed with a diaminobenzidine chromogen which was catalyzed by streptavidin-Horseradish peroxidase from the kit. Streptavidin-HRP and 3,3-DAB were used according to the manufacturer's instructions (DABmap detection kit, Ventana Medical Systems). Finally, sections were counterstained with Gill hematoxylin and sodium bicarbonate. Each section was scanned at a high resolution (40X) using the Nanozoomer Digital Pathology equipment (Hamamatsu, Bridgewater, NJ).

Manual immunohistochemistry

Manual immunohistochemistry (IHC) visualization of APLNR was done using Novolink TM Max Polymer Detection System (Leica, RE7280-K) as mentioned in the procedure recommended by the manufacturer. Briefly, 4 µm FFPE sections of MCF-7, HEK293 cells, ER^+ breast carcinoma, thyroid and muscle tissues were cut and dried at 62°C for 30 minutes, deparaffinized in xylene 100 % and rehydrated through graded alcohols baths. After a wash in deionized water, antigen retrieval for primary antibody use was performed in boiling EDTA buffer (pH 9.0) at 97°C for 1 hour. After cooling in de-ionized water, endogenous peroxidase activity was neutralized using a peroxidase block solution for 5 minutes with constant double washing by Tris Buffer Saline for 5 minutes. Nonspecific binding of IgG was blocked using Protein Block solution (Novolink TM) for 5 minutes. The sections were incubated with the anti-APLNR primary antibody (Santa Cruz Biotechnologies, CA, USA, 3C3-7, sc-517300), for 1 hour at room temperature, in a humidified chamber and then, they were incubated with Novolink TM Polymer 30 minutes. Staining was developed with 3, 3′-diaminobenzidine (DAB) working solution for 5 minutes and washed with distilled water. Finally, counterstaining was performed for the sections with hematoxylin. The sections were mounted with cover slides.

Digital image analysis of immunohistochemistry immunostaining

Quantitative analysis of APLNR IHC staining was performed on digital microphotographs obtained from representative imaged areas as magnified at x40 of MCF-7 pellets, HEK297 pellets, ER^+ breast adenocarcinoma and normal smooth muscle tissue (32 bits RGB images, 3384 × 2708 pixels, area of 1.267 mm2). Determination of the distribution of APLNR staining in tumor cells was implemented with the open-source image analysis QuPath software developed by Dr. Pete Bankhead and generously made available to the biomedical community as freeware (23). Briefly, APLNR analysis was performed in annotated areas of enriched cellularity with a density of more than 100 cells for MCF-7 cell lines and controls using Qupath's Cell and Membrane command, which identify a whole cell, nuclei, cytoplasm, and membrane compartments. Mean measurement detection was carried out by Cell: DAB OD mean, Cytoplasm: DAB OD mean, Nuclei: DAB OD mean and Membrane: DAB OD mean command respectively, and DAB was defined as the presence of any discernible DAB positivity in different compartment either punctate or diffuse. Intensity thresholds for DAB measurements were applied by Segmentation classifier command based on the application of machine learning algorithms and dispensed compartments with positive versus negative decisions per cell, nucleus, cytoplasm, and membrane based on immunostaining intensities on a continuous scale. The number of positively stained compartments detected was represented as the average number of positive compartments per mm2. The results were also shown with highlighted images of detected cells, nuclei, membranes, and cytoplasm. The percentage of positive data was extracted from each area and averaged across replicates.

Fluorescence staining and confocal microscopy

Indirect immunofluorescence staining for APLNR was performed in MCF-7 cells cultured under starvation. MCF-7 was maintained under estrogen starvation in the growing medium in plated a six-well culture plate containing sterile coverslips at 0.5 $x10^6$ cells per well, culture in a humidified 5% CO_2 atmosphere at 37°C until they reached 80% confluence. After three days of culture, cells were washed three times with 1x PBS for 5 minutes each and then fixed immediately with freshly prepared 4% paraformaldehyde (Sigma-Aldrich, 158127), at room temperature for one hour. Cells were permeabilized with 0.2% Triton X-100 (Fisher Scientific, 9002-93-1) in Phosphate Buffered Saline, for 1 min at room temperature. After three times of washes with wash buffer (0.5% BSA, 0.05% Tween 20 in PBS), nonspecific antigens were blocked with blocking buffer (5% BSA, 0.05% Tween 20 in PBS) for two hours at room temperature. After 3 more washes in 1x PBS at 5 minutes per wash, cells were incubated with 1:100 primary monoclonal mouse anti-human APLNR antibody (Santa Cruz) diluted in antibody buffer (1% BSA, 0.1% Tween 20 in PBS) overnight at 4 °C in a moist chamber. Three times washes were repeated as mentioned above. The cells were incubated with a 1:500 FITC-conjugated secondary antibody for one hour at room temperature.

Control cells without primary antibodies were included as a negative control for the nonspecific binding of the secondary antibody. After a final triple-washing step, the cells were rinsed with PBS. Cells were again washed 3 times in 1X PBS for 10 minutes per wash, then incubated for 20 minutes with a 1:2,000 DAPI nuclear stain, washed again, and the coverslips air-dried. A drop of Slowfade Light antifade reagent glycerol buffer was added to the cells, which were then mounted on glass slides. Fluorescent images of samples were captured using a confocal microscope (Zeiss confocal microscope LSM 700) at the Institute for Research in Immunology and Cancer (IRIC) (Université de Montréal, Montréal, Québec), with 63x /1.4 Plan Apo DIC lens. Photomicrographs were taken with a 40X magnification objective lens. Images were processed with Metamorph.

AlamarBlue assay

MCF-7 cells cultured, as mentioned in the cell culture section, were harvested and subsequently counted for serial dilutions to prepare 160 µL of cell suspension with different cell densities, ranging from 1000, 2000, 3000, 4000 and 5000 cells/well. The resulting cell suspensions were seeded into triplicate wells of a 96-well clear flat-bottom polystyrene TC-treated microplates (Corning Costar, Catalog no.: 3596) and cells were kept in a humid atmosphere incubator at 37 °C and 5 % CO_2. After an initial 24 h period to allow cell attachment, the cells were treated or tested, and consecutive measurements were made each day. After exposure, the medium was removed. The wells were filled with 160 µL of fresh media, which were supplemented with a 4% concentration of resazurin at 20 % (v/v) of stock AlamarBlue® solution to medium as indicated as mentioned by the manufacturer's protocol. As the dye is light-sensitive, all steps were performed under light protection, and the plates were wrapped in Aluminum foil and were kept for four h in a CO_2 incubator in a humidified environment at 37 °C under similar conditions as used during routine cell growth and maintenance. Controls were performed as mentioned by the manufacturer and were added before measurements in triplicate to empty wells. The negative control was represented by 160 µL from the medium exempt from cells, whereas the positive control was prepared by incubating a 2 % AB/Medium solution at 95°C until obtaining a 100 % reduced form. After a further incubation of the plate for 3 hours at 37°C, the fluorescence readings from every well were measured and recorded at the indicated times in a 96-microplate reader (FlexStation II, molecular devices), the excitation wavelength was set at 530 nm, emission wavelength was set at 590 nm, using the SoftMax software (Molecular Devices, California, USA). The number of viable cells correlates with the magnitude of dye reduction and is expressed as a percentage of AB reduction (23-25). The calculation of the percentage of AB reduction (%AB reduction) was done according to the manufacturer's protocol. The results are presented as a growth rate (percent of AlamarBlue signals in a given time to percent of AlamarBlue in the vehicle at one day zero).

Lysotracker labeling

MCF-7 cells with or without treatment were loaded with 50 nM Lyso-Tracker Green (LTG) (L7526, Invitrogen) according to the manufacturer's instructions by incubating cells with dye for 1 h at 37°C. Briefly, a cell monolayer cultured on a coverslip in 6 well Petri dishes was washed with PBS 1X three times. LTG was loaded at 50 nM and cells were then washed. MCF-7 cells were incubated in 400 µL of PBS 1X in the presence of the DNA viability dye, 4',6-diamidino-2-phenylindole (DAPI; 200 ng/mL; cat. no. D9542, Sigma Chemicals, Poole, UK). MCF-7 was fixed by PFA. Confocal images were collected with a Zeiss LSM 700 inverted laser scanning confocal microscope (Carl Zeiss; Oberkochen, Germany) using 63X oil 1,4 N.A. Planapo 63x objective lens. LTG signals were excited at 488 nm and data was then analyzed on DAPI versus Fluorescence signals. LTG signals from samples were then compared by histogram analysis of the mean fluorescence image (MFI). LTG MFI upregulation from autophagy-induced samples and untreated cells were compared to show the average fold increase and the individual data points shown. About 3 independent experiments were collected.

Quantitative analysis of immunofluorescence

The Qupath software (University of Edinburgh, https://qupath.github.io) was used to determine the ration of pixels presenting Lysotracker signals and DAPI signals, in the image scatter diagram.

Whole-cell lysis and cytosolic fraction

Experiments were performed with estrogen-starved MCF-7 cells cultured in 6-well plates. For treatment, cells were incubated with vehicle (untreated cells), 100 nM of apelin-13 alone, or associated with 1 nM of 17β-estradiol (E2) for 5, 10, 20, 30, and 60 minutes. After treatment with the indicated agents, the medium aspired, and the cells were washed 3 times with ice-cold PBS. For whole-cell extraction, cells were directly lysed in 100 µL of lysis buffer (50 mM Tris-HCl, pH 7.5, 150 mM NaCl, 5 mM ethylenediaminetetraacetic acid (EDTA), 2% sodium dodecyl sulphate (SDS), 0.5% Triton, 1% NP40) containing the protease inhibitors, dithiothreitol (1 mM), aprotinin (1 mg/mL), leupeptin (1 mg/mL), phenylmethylsulfonyl fluoride (PMSF) (0.3 mM), NaF (1 mM) and sodium orthovanadate (1 mM). For the cytosolic fraction, cells were lysed in lysis buffer (10 mM PIPES 5 mM, pH 8.0, 2 mM KCl and 0.5% NP-40), containing protease inhibitors, dithiothreitol (DTT) (1 mM), aprotinin (1 mg/ mL), leupeptin (1 mg/ mL), PMSF (0.3 mM) and DTT (1 mM). After resuspension in lysis buffer, cells were then scraped with a tissue culture cell scraper and collected in centrifuge tubes. Cell lysates or cytosolic fractions were immediately sonicated for 15 minutes at 4°C (Bioruptor, Diagenode). Then, the cells were allowed to lyse for 10 minutes at 4 °C. Lysates were then centrifuged in 1000 g for 10 min at 4 °C. Cytosolic fractions were obtained from the supernatant. Lysates were boiled in Laemmli solution 6X (375 mM Tris-HCl pH 6.8, 9% SDS, 50% glycerol, 10% beta-mercaptoethanol, 0.03% bromophenol blue) for 5 min at 95°C and were centrifuged for 5 min. Protein concentration in whole-cell extracts and cytosolic fractions supernatants were determined using the Lowry method, as described in the manufacturer recommendations (Biorad, Mississauga, ON, Canada).

Immunoblotting analysis

Whole-cell and cytosolic fractions were subjected to

7% sodium dodecyl sulfate-polyacrylamide electrophoresis (SDS-PAGE, 8% acrylamide) and equal protein amounts 30 µg by sample per well. Proteins were separated by electrophoresis at 100-150V for 60 minutes and transferred to polyvinylidene fluoride (PVDF) membranes (EMD Millipore) for 2 hours at 100V using a Trans-blot apparatus (Bio-Rad, Mississauga, ON, Canada). The membranes were then blocked for 1 hour at room temperature with 5% w/v skimmed milk in 1X Tris-Buffered Saline with Tween-20 (TBST; 500 mM NaCl, 20 mM Tris–HCl, pH 7.6, 0.05 % (w/v) Tween 20). The membranes were then washed three times in Tris buffer solution with 5% tween 20 (5 min per wash) prior to being incubated overnight at 4°C with the appropriate primary antibody under gentle agitation at 4°C in a blocking buffer. Non-conjugated rabbit primary antibodies (AMPK-α, phospho-AMPK) were used at 1:200 in a mixture with a primary mouse monoclonal-FITC conjugated antibody raised against human α-tubulin (1:5000 dilution) as a loading control, whereas APLNR-antibody was used at 1:100. These membranes were washed three times for 3 min in TBST and incubated with an HRP-conjugated goat anti-rabbit Ab (Bio-Rad) (1:5000 dilution) in blocking buffer for 1 h with gentle agitation at room temperature. Membranes were removed from the primary antibody solution and washed three times in PBS-T solution. After washing, membranes were incubated with 0.5× blocking solution + 0.1% Tween-20 + 0.01% SDS containing a Goat Anti-Rabbit HRP-Conjugated Antibody (Jackson ImmunoResearch; #111-035-144, 1:10,000) or anti-mouse for 1 hour at room temperature. Membranes were removed from the secondary antibody solution and washed for 5 minutes in 25 mL of TBS-T. Membranes were covered with the Clarity western ECL substrate chemiluminescent detection reagent (Bio-Rad) for 5 min according to the manufacturer's instructions (Thermo Fisher Scientific) before image acquisition. Imaging was performed using dual chemiluminescent and fluorescent exposures which were captured on a ChemiDoc MP Imaging System (Bio-Rad Laboratories Inc.); with "Chemi Hi-Resolution" settings (2×2 camera binning). Exposure times were set automatically with ChemiDoc™ MP Imaging System (Bio-Rad Laboratories Inc.) The developed signals of blots were then analyzed by the Image Lab software to obtain densitometry values. The blots are representative of three independent experiments and bar diagrams are included showing the quantification of western blot signals.

Statistical analyses

All statistical analyses were carried out using Prism 8.0.1 GraphPad Prism (GraphPad Software Inc, USA). Statistical significance was considered, with a *p-value* less than 0.05.

Results

Expression of APLNR by the human breast cancer cell line MCF-7

To validate the specificity of the IHC reaction for the APLNR protein using the C3C-7 antibody (Santa Cruz Biotechnology), staining was first performed using as positive controls an ER$^+$ breast carcinoma tumor (Fig. 1A) and normal thyroid tissue (Fig. 1B). Sections from smooth muscle chosen as a negative control (26) remained entirely negative (Fig. 1C). Similar results were obtained in IHC analysis performed using HEK293 cells (Fig. 1D), which are known not to express APLNR mRNA and protein (27). Paralleled digital image analysis of the same sections by QuPath (Fig. 1A, 1B, 1C, and 1D) demonstrated almost no APLNR staining in both smooth muscle cells and HEK293 cells, as well as different expression levels in expressing ER$^+$ breast carcinoma and thyroid (mention color code).

IHC was then used to assess the expression of the APLNR protein in pellets of freshly harvested MCF-7 cells (Fig. 2A). Using QuPath, APLNR staining in MCF-7 cells cultured under estrogen starvation was detected as heterogeneous since 74% of the cells failed to demonstrate any APLNR reactivity (Fig. 2B). However, a minority of MCF-7 cells (26%) cells appeared to stain positively. Applied texture-based analysis of the cell staining demonstrated more varied expression levels (Fig. 2B) and allowed for their classification as follows: negative cells with a complete absence of staining (50%), faint staining (+, 20 %), moderate staining (++, 25 %) and intense staining (+++, 18 %). Indeed, APLNR shows a dotted expression pattern, present only in the nucleus or the cytoplasm, whereas no expression at the cell membrane was detected in any of the cells (Fig.2C). APLNR receptor expression was also explored in adherent MCF-7 cells using confocal microscopy. MCF-7 cells were subcultured under estrogen starvation to form a monolayer and subsequently were fixed for imaging. The results from this confocal microscopy analysis showed a tight monolayer of MCF-7 cells with a homogenous expression of actin filaments

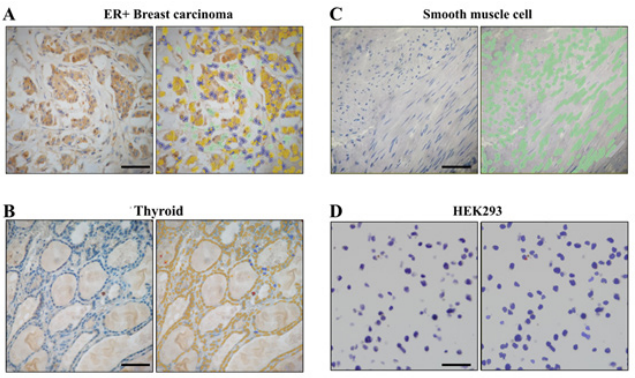

Figure 1. Immunohistochemical validation of the APLNR antibody in human tissue and cell line. Typical expression pattern of APLNR in ER$^+$ breast carcinoma (epithelial cells) (A) and in epithelial thyroid cells (B). Whereas no APLNR staining was detected in smooth muscle cells (C) and HEK293 cell line (D). Scale bars, 50 µm. **(A).** IHC analysis by Qupath (Left) of APLNR+ Breast carcinoma tissue photomicrographs (Right) show heterogenous expression of the APLNR receptor with positive "yellow" and negative "blue" expressing epithelial cells. Stromal cells and fibroblasts are shown with "green" color. Scale bars, 50 µm. **(B).** IHC analysis by Qupath of APLNR+ in thyroid tissue photomicrographs shows the expected positive expression of the APLNR receptor in follicular cells as indicated with "Yellow" for positive APLNR expressing cells. Few cells show negative expression "Blue". Scale bars, 50 µm. **(C).** IHC analysis by Qupath of APLNR+ in smooth muscle tissue photomicrographs show the expected negative expression of the APLNR receptor in smooth muscle cells as indicated with "Green" for negative APLNR expressing cells. Scale bars, 50 µm. **(D)** Typical negative expression pattern of APLNR was detected in HEK293 cell line with no APLNR staining "Blue". Scale bars, 50 µm.

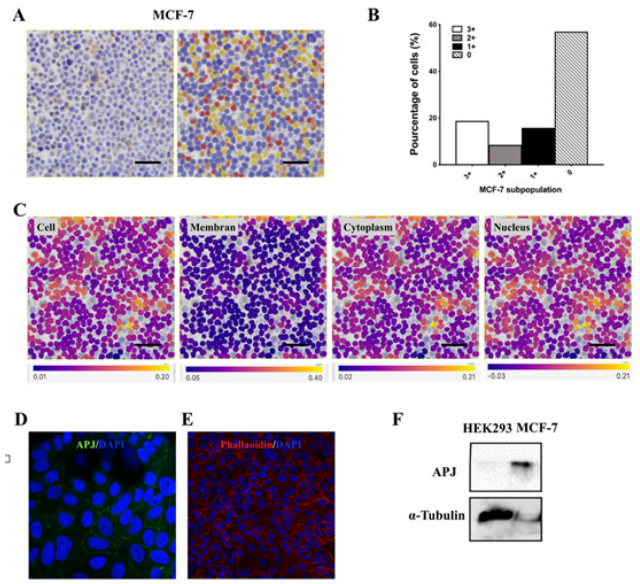

Figure 2. Expression of the APLNR in MCF-7 cells. (A). IHC analysis by Qupath shows the expected expression of the APLNR receptor in MCF-7 cells with a heterogeneous pattern of immunoreactivity in these cells. "Blue" indicates negative APLNR expressing cells, "yellow" for moderate expressing APLNR cells, and "red" for APLNR expressing cells. Scale bars, 50 µm. **(B).** Statistical measurements detected in (A) allowed classifying MCF-7 on different subpopulation according to the DAB intensity signals in the whole-cell and showed as plots of cells scored as 1+, 2+, and 3+ positive cells or 0, negative cells. **(C).** Subcellular localization of APLNR in MCF-7 cells estimated by Qupath and presented as heat maps for whole-cell, membrane, cytoplasmic, and nuclear localization. Whereas no DAB signals are detected in the membrane, the detected APLNR seems to be distributed in cytoplasmic and nuclear localization. Scale bars, 50 µm. **(D).** Dual fluorescence was performed in MCF-7 monolayer assessed in permeabilized cells with mouse APLNR antibody visualized with Alexa 488 anti-rabbit secondary antibody (green) and the nuclear staining dye DAPI. Images obtained are representative of 50-100 cells per experiment repeated three independent times and viewed at 40X magnification using a Carl Zeiss LSM 700 laser scanning confocal microscope. **(E).** Confocal microscopy of MCF-7 monolayer cultured on the coverslip, stained for phalloidin (red), and DAPI (blue). The image shown is representative of 50-100 cells per experiment viewed at 20X magnification using a Carl Zeiss LSM 700 laser scanning confocal microscope. **(F).** Western blot analysis of MCF-7 cell extracts was performed using antibodies specific for APLNR receptor and α-Tubulin. Extracts from HEK293 cells were used as negative control.

as shown by phalloidin staining (Fig. 2D). APLNR staining was detected as continuous and boarding the cell surface in almost all cells, indicating that adherent MCF-7 cells express APLNR at the plasma membrane. APLNR expression was also detected in MCF-7 cells by Western blot analysis, yielding a band with an MW of 50 kDa band (Fig. 2E). As expected, no band was detected in lysates of HEK293 cells, which do not express APLNR (Fig. 2F). Together, our results demonstrate that MCF-7 cells express APLNR, which is located at the cell surface when cells form a monolayer in the absence of estrogens.

Apelin-13 induces the proliferation of MCF-7 cells under estrogen deprivation which is abolished by E2 treatment

To investigate the functionality of APLNR, we analyzed proliferation rates of MCF-7 cells cultured in the presence or absence of apelin-13 using the AlamarBlue assay. First, the optimum cell plating density for which a linear response relating cell numbers to AlamarBlue reduction fluorescence was assessed for a short culture time (5 days) in the absence of any treatment. Data shows that AlamarBlue readings were precisely proportional to the cell seeding numbers with a seeding density ranging from 1000 to 5000 cells/well (Fig.3A). Using 1000 cells/well as a seeding density, cells cultured under estrogen-depleted conditions were treated with increasing concentrations of apelin-13 (0,1, 1, 10, 100, 1000 nM) and the proliferation rate was assessed for the indicated time points (Fig.3B). The doubling rate of cells treated with the vehicle only was 3 days. In the presence of 0.1 nM, 1 nM, and 10 nM apelin-13, no change for the doubling growth rate in comparison to the vehicle was achieved. However, the addition of apelin-13 at 100 nM and 1000 nM to the estrogen-depleted medium resulted in a marked increase in the MCF-7 cell proliferation rate. Alamar blue readings were significantly increased from day 2 for cells treated with 100 nM apelin-13, and from day 1 for cells treated with 1000 nM apelin-13 (Fig.3B). Our data thus indicates that apelin-13

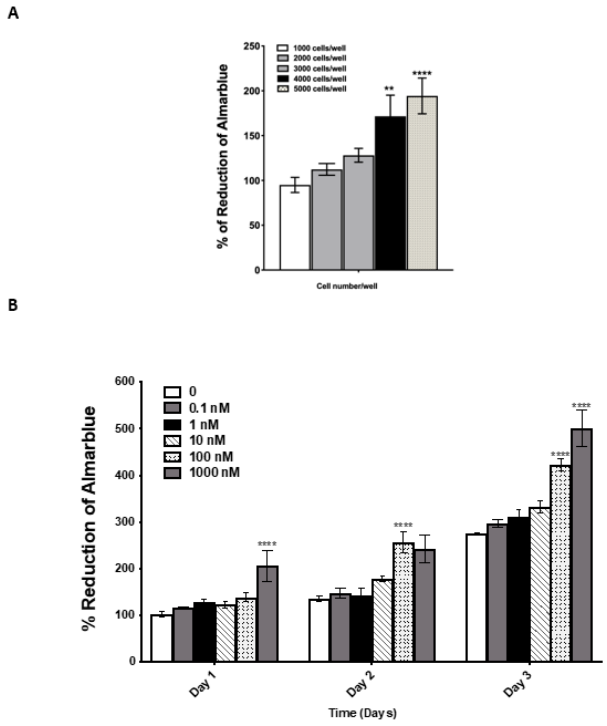

Figure 3. MCF-7 cell growth was significantly enhanced following apelin-13 treatment in a concentration dependent manner under estrogen starvation. A. AlamarBlue reduction was proportional to the cell seeding number with a seeding density ranging from 1000 to 5000 cells/well. The experiments were performed four times and each independent experiment consisted of two to three measurements. Statistical analysis was performed using one-way repeated measures ANOVA followed by Dunnett's post-test against the smallest cell concentration/well, ** $P \leq 0.01$, and **** $P \leq 0.0001$. **B.** Increased concentrations of apelin-13 were separately applied to MCF-7 cells under estrogen free condition. The cells were incubated for 1, 2, or 3 days. Effects of apelin-13 on MCF-7 cell viability were determined using Alamar blue assay. The experiments were performed three times and each independent experiment consisted of three to four measurements. Statistical analysis was performed using two-way repeated measures ANOVA followed by Dunnett's post-test against the control sample, ** $P \leq 0.01$, *** $P \leq 0.001$, and **** $P \leq 0.0001$.

efficiently enhanced MCF-7 cell growth in a concentration-dependent manner.

We then investigated the effects of co-treatment with E2 and apelin-13 on cell proliferation. Consistent with the previous results, treatment with apelin-13 increased the proliferation rate of MCF-7 cells at one day, three days, and five days (100, 200, and 400%, respectively), in comparison to the control cells (Fig.4). Similarly, E2 (1 nM) increased the growth rate of MCF-7 cells at 1, 3, and 5 days (100 %, 200 %, 400 %, respectively) in comparison to the control cells (Fig.4). However, no difference in MCF-7 proliferation rate between control and MCF-7 cells co-treated with E2 and apelin-13 was observed for one day, three days or five days, indicating that the combination of E2 and apelin-13 did not affect the growth rate of MCF-7 cells. Thus, our data indicate that apelin-13 efficiently enhanced MCF-7 cell growth in a time-dependent manner and that E2 abrogated the apelin-13-induced effect on MCF-7 cell growth rate.

Both apelin-13 and E2 suppress autophagy in MCF-7 cells under estrogenic deprivation

Autophagy can be monitored by Lysotracker, a specific probe for lysosomes, which can be imaged by confocal microscopy (28). To assess the basal autophagic flux, the accumulation of puncta signals was monitored in estrogen-deprived cells treated with the vehicle at three and 24 hours. The fluorescence of Lysotracker was distributed in a punctate pattern in MCF-7 starved cells, corresponding to the normal lysosomes' organelle localization and distribution. Lysotracker signals were quantified. In the absence of any treatment, significant enhancements of twenty-fold in puncta numbers and signals were detected in the control cells at 24 h compared to 3 h (Fig.5A). This data indicate that estrogen starvation led to a progressive autophagy increase, as observed between 3h and 24 h.

As expected, when MCF-7 cells were exposed to apelin-13 for three hours, a drastic decrease in lysotracker signals and puncta formation was observed, and this effect was maintained over 24h. A similar pattern of fluorescence in cells treated with E2 was observed. However, consistent with the antagonistic action of combined E2 and apelin-13 treatment, MCF-7 cotreated with E2 and apelin-13 did not exhibit a change in puncta signals in comparison to vehicle-treated cells. The decrease in the lysotracker signals is consistent with autophagy inhibition (Fig.5B). Our

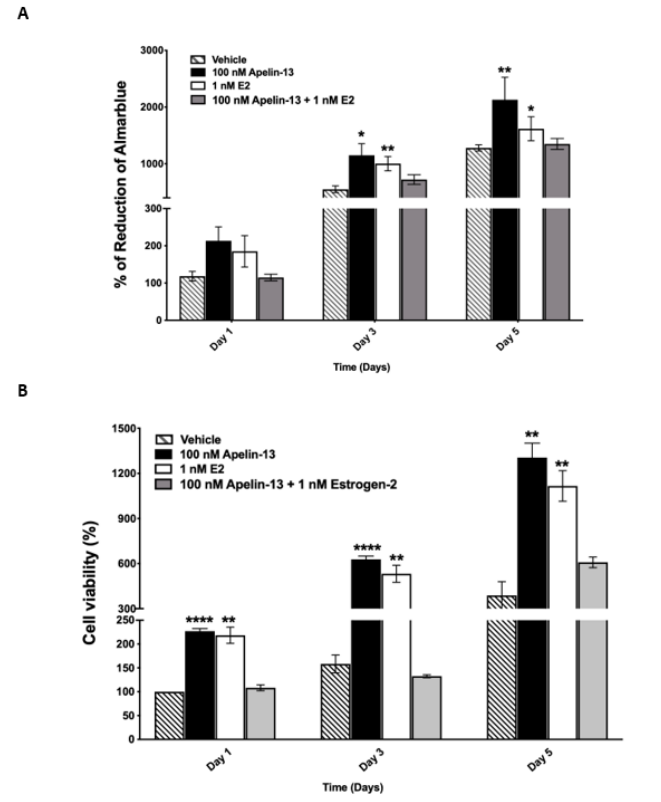

Figure 4. Effect of apelin-13 on MCF-7 viability in the presence or absence of Estrogen. A. MCF-7 cells maintained in the absence of estrogens for three days were treated with apelin-13 (100 nM), in the presence or absence of estradiol (E2, 1 nM). The cells were incubated for 1, 3, or 5 days. Effects of apelin-13 and E2 on MCF-7 cell viability were determined using Alamar blue assay. Statistical analysis was performed using two-way repeated measures ANOVA followed by Dunnett's post-test against the control sample, * $P \leq 0.05$, ** $P \leq 0.01$, and **** $P \leq 0.0001$. **B.** Trypan blue exclusion assay of MCF-7 cells treated with apelin-13, E2 or apelin and E2. The results are presented as the number of viable cells counted per well and the percent of viable cells relative to untreated control. The viability of untreated control cells was taken as 100 %. Results are presented as means compared to the control as tested by the Student's t-test.

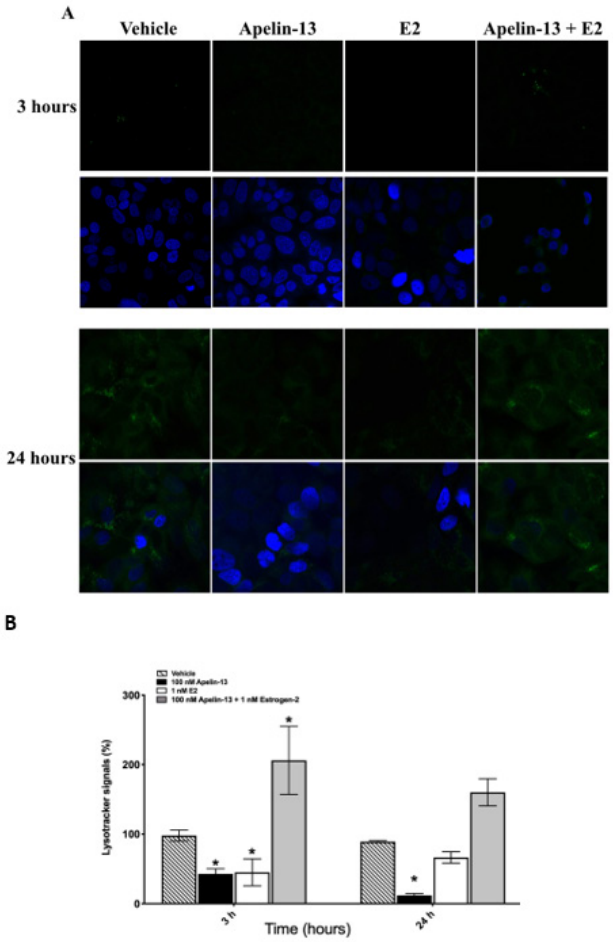

Figure 5. Lysotracker in MCF-7 cell lines is decreased by apelin-13. A. Lysosomes in MCF-7 starved cells were visualized by confocal microscopy after their labeling with LysoTracker ® (Green fluorescence). MCF-7 cells were treated with apelin-13 (100 nM), 1 nM E2 (1 nM), combination of (100 nM apelin-13 and 1 nM E2) or vehicle for 3h or 24 h, then fixed and imaged by confocal microscopy. The images are representative of 50 cells from the adherent monolayer on the coverslip from three independent experiments. **B**. The intensity of the LysoTracker staining was quantified by Qupath (Magnification: 40×).

results confirm that the cotreatment of MCF-7 cells with apelin-13 and E2 reduces their sensitivity to the inhibitory actions of both molecules on autophagy. Collectively, these results indicate that both apelin-13 and E2 abrogate autophagy-induced starvation.

Variation in the cellular level of APLNR according to the type of activation

Ligand-receptor internalization and trafficking are traditionally considered part of the cellular desensitization after receptor activation, whereby signaling by the activated receptor are abrogated and the receptor itself is degraded or recycled back to the membrane. In the presence of apelin-13, a rapid increase of APLNR protein level occurred in cytoplasmic enriched fractions within 5 min followed by a consistent decrease in this compartment (Fig. 6A). It is to be noted that the cytosolic contents of APLNR receptor in MCF-7 cells treated by combined E2 and apelin-13 showed a similar transient increase of the amount of APLNR after 5 minutes but then regained about the initial level and remained approximately constant and no subsequent decrease was documented throughout one-hour treatment. This result suggests that APLNR protein levels are exposed to a rapid regulation by apelin-13 and that this regulation is reversed by E2. Indeed, this result supposes that ER is involved in the effects of apelin-13 and indicates that crosstalk occurs between APLNR and ER.

Association between APLNR activation and AMPK phosphorylation

Apelin-13 decreases the autophagy in MCF-7 under estrogen starvation which indicates that a cascade of signaling pathways has been involved beyond APLNR activation. The AMPK pathway was explored since this pathway is known to be a common regulator of autophagy and cell proliferation in MCF-7 cells and it could be altered by apelin-13. Western blotting for phospho-AMPK was performed in MCF-7 cells incubated in serum and estrogen-free medium with apelin-13 treatment in the presence or absence of E2. After serum and estrogen starvation, the intensity of the phosphorylated-AMPK was detectable, but a significant fraction became dephosphorylated by apelin-13 in a time-dependent manner. The phosphorylation levels of the Thr172 residue, an activator site of the AMPKα subunit required for its enzyme activity, were rapidly, drastically decreased, reaching 50 % ± 5.2% at five min compared to untreated control cells (Fig. 6A) and a minimal level at 30 min after treatment (Fig.6A). This decrease was stably maintained for over 1 hour. No detectable difference was seen in the total AMPK between each of the cell lines (Fig. 6B). Indeed, cotreatment with apelin-13 and E2 did not permit to recover of the level of phosphorylated AMPK to a basal level and show a similar profile of dephosphorylation. Collectively, these results suggest that dephosphorylation of AMPK could be implicated in apelin-mediated effects on MCF-7 cell proliferation regardless of the presence of E2. This result suggests that crosstalk between ER and APLNR receptor include at least the AMPK pathway.

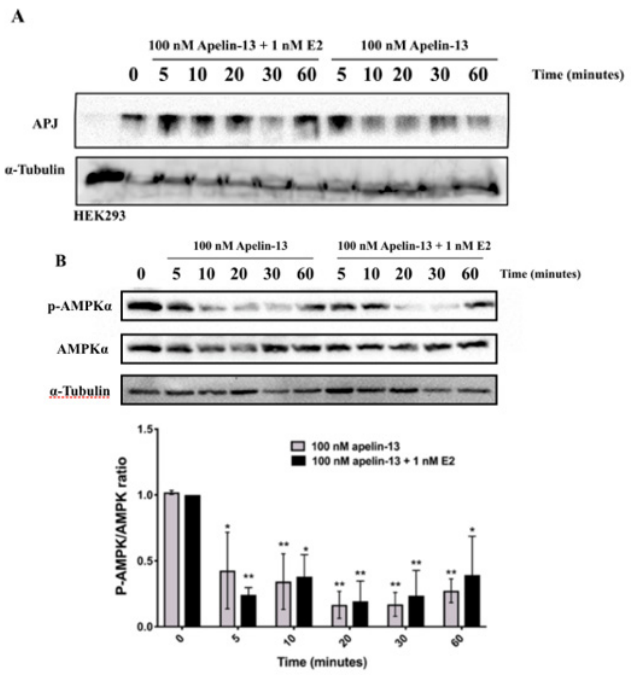

Figure 6. Short-term effects on APLNR signaling in MCF-7 cell lines under estrogen starvation were reversed by E2. A. MCF-7 cell lines were exposed to a concentration of 100 nM of apelin-13, for the indicated times, in the presence or absence of 1 nM estrogen-2. Western blot analysis of MCF-7 cells extracts was performed using antibodies specific for APLNR receptor and α-Tubulin. HEK293 cell line extracts were loaded as a negative control for APLNR expression. Proteins of a mixed three independent experiments was loaded. **B.** MCF-7 cell lines were exposed to a concentration of 100 nM of apelin-13, for the indicated times, in the presence or absence of 1 nM estrogen-2. Western blot analysis of MCF-7 cells extracts was performed using antibodies specific for phospho-AMPK-α (Thr172), total AMPK-α and α-Tubulin. Detected signals of phospho-AMPK-α and AMPK proteins were normalized to α-Tubulin. AMPK activity was represented as the ratio of phospho-AMPK-α to total AMPK-α normalized to the untreated cells (time 0). Error bars represent means ± SEM of 3 independent experiments. Statistical analysis was applied using one-way ANOVA with Dunnett's post-test against the untreated cells. * $P \leq 0.05$, ** $P \leq 0.01$.

Discussion

The exploration of the mechanisms of resistance to endocrine therapy in ER$^+$ cells has led to the identification of several molecules, in particular adipokines that act in concert with, or independently from, estrogenic signals thereby promoting the growth of tumor cells (29, 30). The adipokine apelin has been extensively studied for its growth-promoting effects on different tumors, including breast cancer cells (20, 31). However, much is still unknown about the underlying mechanisms of apelin-mediated activation in these cells whereas the expression and functional role of apelin and its receptor in normal and malignant breast cells remain to be investigated. Recently, it has been shown that apelin induces the proliferation of the ER$^+$ cell model, and MCF-7 cell lines (21). The results from the present study demonstrate the expression of APLNR in the MCF-7 cell line and explores possible underlying mechanisms driven by APLNR activation that promote the growth rate of MCF-7 cells under estrogen starvation.

Using three independent methods, IHC, confocal microscopy, and Western blot analysis, the constitutive expression of APLNR on MCF-7 cells cultured in the presence of estrogen was confirmed. The specific detection of the APLNR by the C3C clone antibody was validated,

supporting its suitability for clinical use in IHC tests. Antibody specificity was also confirmed by the detection of the APLNR protein, despite preanalytical variability that can influence the subcellular localization of plasma membrane proteins in MCF-7 cells (32). Consequently, the distribution pattern of APLNR differed according to the technique of detection used. Using IHC, APLNR immunoreactivity was observed with a punctate aspect in the cytoplasmic compartment, whereas no discernible localization at the membrane was detected at the cell membrane. In contrast, however, with confocal microscopy, APLNR staining was homogenously detected at the cell surface, with a staining pattern typical of GPCRs (33). This discrepancy can be explained by the treatment of the cells with trypsin, used for harvesting MCF-7 cells. Indeed, trypsinization is known to induce modification of cell surface molecules implicated in the MCF-7 cell growth. It has been shown that the proteolytic activity of trypsin during cell culture may cleave the cell surface growth factor receptors or membrane proteins (32). Thus, it is possible that subsequent internalization of the APLNR had occurred following MCF-7 cell trypsinization reminiscent of that observed with GPCRs (33, 34). In contrast, APLNR staining for confocal microscopy was performed without trypsin treatment: MCF-7 cells were directly fixed in their adherent state, forming a monolayer, thereby conserving their protein distribution. Our results demonstrate that APLNR is constitutively expressed at the cell surface of MCF-7 cells and harvesting by trypsin is likely to alter its membrane localization, possibly by internalization of the receptor. Further experiments should help clarify this hypothesis. Nevertheless, to our knowledge, this is the first observation that reported APLNR expression in ER^+ breast cancer cells.

In order to explore the functionality of the APLNR and its role in apelin-13-mediated breast cancer cell responses under estrogen starvation, changes in AMPK activation and autophagy were explored. The growth rates of short-term MCF-7 starved cells observed in these experiments are concordant with the rates reported in the literature (35) representing approximately a doubling time of growth at three days was found to be effectively enhanced by apelin-13. Those results also highlight that because of the constitutive expression of APLNR by MCF-7 cells, the growth-promoting effects of apelin-13 can be detected within five days. They furthermore show that estrogen deprivation does not affect the ability of apelin to maintain the growth of MCF-7 previously demonstrated in our results in the presence of exogenous estrogen. Future reports should be carried out to confirm the mitogenic properties of apelin-13 is healthy and tumor cells are given its presence in mammary tissue (36).

The aforementioned results highlight a possible connection between autophagy and cell growth in estrogen-starved breast cells in the presence of apelin-13. Concomitant inhibition of autophagy and enhanced growth in the apelin-13-treated cells suppose that autophagy regulating pathways are mobilized in MCF-7 triggering APLNR activation at least by controlling the basal autophagic flux. AMPK is by far the most studied kinase related to autophagy regulation (29, 37, 38). Although the link between AMPK and autophagy is established, upstream regulators of AMPK in the context of autophagy response are still largely unknown. The Association of decreased activation of AMPK and autophagy with enhanced tumor cell viability raises several questions regarding the mechanism by which apelin-13 can activate tumor growth under estrogen starvation. It is essential to characterize upstream signaling pathways implicated in APLNR-mediated activity in MCF-7 cells. The observations in this study indicate that under estrogen starvation, AMPK is constitutively activated in MCF-7, which is consistent with numerous studies (39, 40). Indeed, the latter kinase becomes rapidly deactivated by apelin-13, which could be attributed to a direct consequence of APLNR activation. Thus, the APLNR-AMPK axis seems to be a short-term mobilized pathway, consistent with a GPCR rapid signaling. AMPK deactivation by apelin-13 may be explained by post-translational modifications that lead to dephosphorylation of a threonine residue (T172) in the loop of the catalytic α-subunit which constitutes a prerequisite for the antiproliferative activity of AMPK as reported in the literature (41). The decline in AMPK deactivation is strongly associated with the development and progression of cancer. Indeed, a large number of reports strongly support the anti-proliferative function of activated AMPK in MCF-7 (39) which is corroborated by the notion that it is activated by many anti-cancer therapy molecules that induce apoptosis and survival inhibition such as Rhus verniciflua extract (42), Quercetin (43), Compound K (44), Metformin (45), AICAR (46), *Citrus unshiu* Peel (47). The results presented here thus are concordant with those pieces of evidence and depict the role of apelin-13 that can restore growth in MCF-7 cells by downregulating AMPK.

Moreover, although all evidence published to date points to the activation of AMPK by apelin-13 (48-50), we show, for the first time, that apelin-13 can also negatively regulate AMPK signaling, via a decrease of its level of phosphorylation. However, it is essential to consider that no previous reports on the interactions between apelin and the AMPK pathway have addressed its effect in breast cells and that apelin-mediated AMPK activation has benne confirmed only in a few studies in human cells, including adipocytes (48), myocardiocytes (49), neural cells (50), human and mouse hepatocyte (51) and HUVEC (52). Furthermore, AMPK activation status by the same hormone seemed to be tissue-dependent as it was verified only for some adipokines, like leptin, adiponectin, and glucocorticoids (53).

In this study, the apelin effect on MCF-7 cell growth was found to be dichotomous and to depend on the presence or absence of estrogen. Hence, the cotreatment of cells with E2 and apelin-13 was expected to show an agonistic effect on the growth rate. However, in contrast, they mutually suppress the effect of each treatment. It is of note that the results from the Lysotracker assay supported identical dichotomy since the association of apelin and estradiol completely abolished the effect of these molecules obtained when applied separately and restored basal autophagy in MCF-7 cells under starvation. The observation that E2 decreased the autophagic flux suggests that in MCF-7 cells, autophagy-regulating pathways are shared between ER and APLNR. Effectively, dichotomous roles of hormones on the growth of breast cancer cell models have been revealed in several studies and were suggested to be related to crosstalk between their respective receptors and the ER (54). A possible role of the unliganded ER, without bound ligand, in modulating responses of other

receptors could be depicted. For instance, this was the case for the insulin receptor (IR), Adiponectin receptor (AdipoR) (10) in a study showing that the AdipoR enhanced following its interaction with the ER in the absence of estrogen in MCF-7 cells. It will be essential to confirm this hypothesis by using a silenced APLNR or ER. Our results propose a possible model to speculate on the differential role of APLNR in MCF-7 growth and suggest an interplay between APLNR and ER (Fig.7). We hypothesize that in the absence of estrogen, sustained apelin-13 levels in the ER^+ breast tumor microenvironment can perpetuate the tumor cell growth. Further experiments are needed to verify and complete his model. Finally, the results from the present study raise the possibility that targeting the APLNR/AMPK axis may represent an attractive strategy to potentiate endocrine therapies for the treatment of breast cancer. In particular, the establishment of anti-APLNR medication for the treatment of hormone-resistant breast cancer is to be proposed given that many active therapeutic agents that modulate APLNR-related pathways are currently being explored for use in clinical trials in different cancer like glioblastoma (54), as well as numerous disorders, including anxiety disorders, bulimia nervosa, and chronic pain (30). More recently, anti-APLNR treatment has been proposed as a nonhormonal therapy for women with menopausal symptoms. Its interest notwithstanding, the use of APLNR-targeting drugs for use in anti-cancer therapy remains experimental. A better understanding of the molecular mechanisms that underlie the role of apelin in breast cancer biology is still necessary for the development of an efficacious anti-cancer therapy.

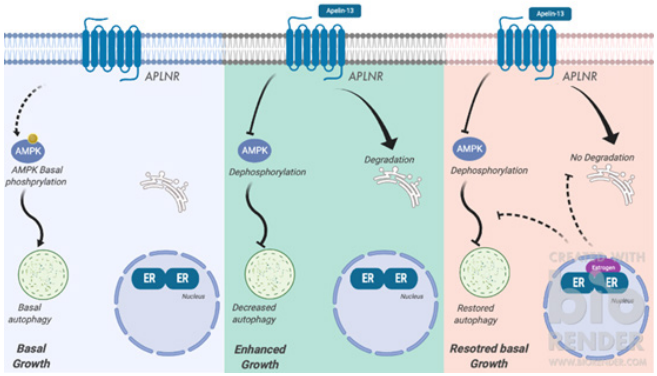

Figure 7. Proposed model for apelin-13 regulation as well as potential crosstalk between APLNR and ER in MCF-7 cells under starvation. Under estrogen starvation (Left cell), unknown upstream signaling activates AMPK constitutively and enhances autophagy to maintain a basal rate of the growth of MCF-7 cells. Activation of APLNR by apelin-13 induces sequential events. APLNR degradation could follow the rapid internalization of this receptor. Indeed, APLNR-dependent signaling deactivates AMPK and thus alter the basal autophagy level and lead to a growth enhancement. However, cotreatment with apelin-13 and E2 may presumably suggest the interaction between ER and APLNR. At least, the level of interaction could be after AMPK deactivation since no modifications of the AMPK phosphorylated level occurred regardless of the presence or absence of estrogen. The first level of interaction proposed is at intermediate events between deactivation of AMPK and autophagy regulation. The second level proposed is at the recycling of the APLNR receptor and preventing complementary pathways more upstream. Thus, interactions between APLNR and ER could be required to link AMPK, autophagy and growth in MCF-7 cells. It will be essential to determine in future experiments by inhibiting the APLNR axis if the APLNR dependent effect is required by exploring: (1) via which signal transduction pathway AMPK is deactivated (2) whether the effect of apelin-13 on breast cancer cells is mediated only by the APLNR or ER ligand-independent effects are necessary. The image was created with Biorender.com.

Abbreviation

AB: AlamarBlue; AdipoR: Adiponectin receptor; APLNR: Apelin receptor; AMPK: Adenosine monophosphate-activated protein kinase; ATCC: American Type Culture Collection; DAB: 3,3'-Diaminobenzidine; DMEM: Dulbecco's modified eagle medium; E2: 17β-estradiol; EDTA: Ethane-1,2-diyldinitrilo-tetraacetic acid; ER: Estrogen receptor; ER^+: Estrogen-responsive breast carcinoma; FBS: Fetal bovine serum; FITC: Fluorescein isothiocyanate; FFPE: Formalin-fixed paraffin-embedded; GPCR: G protein-coupled receptor; HEK293: Human embryonic kidney 293; HepG2: Hepatoma G2; HRP: Horseradish peroxidase; IHC: Immunohistochemistry; IR: Insulin receptor; LTG: Lyso-Tracker Green; MCF-7: Michigan Cancer Foundation-7; MFI: Mean fluorescence image; OD: Optic density; PBS: Phosphate-Buffered Saline; PVDF: polyvinylidene fluoride; SDS-PAGE: sodium dodecyl sulfate-polyacrylamide electrophoresis; TBST: Tris-Buffered Saline supplemented with Tween 20; Thr^{172}: Threonine residue at 172 position

Declaration Of Interests

The authors declare that they have no known competing financial interests or personal relationships that could have appeared to influence the work reported in this paper.

Acknowledgments

The authors would like to thank Dr. Hans Yssel (Sorbonne University, Inserm (CIMI-Paris), Paris, France) for all the corrections suggested and made to the manuscript.

References

1. Murphy C.G. and M.N. Dickler, Endocrine resistance in hormone-responsive breast cancer: mechanisms and therapeutic strategies. Endocr Relat Cancer, 2016; 23(8): R337-52.
2. Bhardwaj P. et al. Estrogens and breast cancer: Mechanisms involved in obesity-related development, growth and progression. J Steroid Biochem Mol Biol, 2019; 189: 161-170.
3. Yamaguchi Y, et al. Detection of estrogen-independent growth-stimulating activity in breast cancer tissues: implication for tumor aggressiveness. Cancer Microenviron, 2014; 7(1-2): 23-31.
4. Horwitz K.B, Costlow M.E, McGuire W.L. MCF-7; a human breast cancer cell line with estrogen, androgen, progesterone, and glucocorticoid receptors. Steroids, 1975; 26(6): 785-95.
5. Comsa, S, A.M. Cimpean, M. Raica, The Story of MCF-7 Breast Cancer Cell Line: 40 years of Experience in Research. Anticancer Res, 2015; 35(6): 3147-54.
6. Blanquer-Rossello, M.D.M, et al. Leptin regulates energy metabolism in MCF-7 breast cancer cells. Int J Biochem Cell Biol, 2016;72: 18-26.
7. Grisouard, J, et al. Targeting AMP-activated protein kinase in adipocytes to modulate obesity-related adipokine production associated with insulin resistance and breast cancer cell proliferation. Diabetol Metab Syndr, 2011; 3: 16.
8. Grossmann, M.E, et al. Obesity and breast cancer: status of leptin

and adiponectin in pathological processes. Cancer Metastasis Rev, 2010; 29(4): 641-53.
9. Liu, Z, et al. Resistin confers resistance to doxorubicin-induced apoptosis in human breast cancer cells through autophagy induction. Am J Cancer Res, 2017;7(3): 574-583.
10. Nepal, S, P.H. Park, Regulatory role of autophagy in globular adiponectin-induced apoptosis in cancer cells. Biomol Ther (Seoul), 2014; 22(5): 384-9.
11. Raut, P.K, et al. Estrogen receptor signaling mediates leptin-induced growth of breast cancer cells via autophagy induction. Oncotarget, 2017; 8(65): 109417-109435.
12. Romero, M.A, et al. Role of Autophagy in Breast Cancer Development and Progression: Opposite Sides of the Same Coin. Adv Exp Med Biol, 2019; 1152: 65-73.
13. Cook, K.L, A.N. Shajahan, R. Clarke, Autophagy and endocrine resistance in breast cancer. Expert Rev Anticancer Ther, 2011;11(8): 1283-94.
14. Maycotte, A. Thorburn, Targeting autophagy in breast cancer. World J Clin Oncol, 2014;5(3): 224-40.
15. Zhou, S.H, et al. Apelin-13 Prevents the Delayed Neuropathy Induced by Tri-ortho-cresyl Phosphate Through Regulation the Autophagy Flux in Hens. Neurochem Res, 2015;40(11): 2374-82.
16. Xie, F, et al. Apelin-13 promotes cardiomyocyte hypertrophy via PI3K-Akt-ERK1/2-p70S6K and PI3K-induced autophagy. Acta Biochim Biophys Sin (Shanghai), 2015;47(12): 969-80.
17. Anagnostou, V.K, et al. Analytic variability in immunohistochemistry biomarker studies. Cancer Epidemiol Biomarkers Prev, 2010;19(4): 982-91.
18. Picault, F.X, et al. Tumour co-expression of apelin and its receptor is the basis of an autocrine loop involved in the growth of colon adenocarcinomas. Eur J Cancer, 2014;50(3): 663-74.
19. Hall, C, et al. Inhibition of the apelin/apelin receptor axis decreases cholangiocarcinoma growth. Cancer Lett, 2017;386: 179-188.
20. Huang, Q, et al. Apelin-13 induces autophagy in hepatoma HepG2 cells through ERK1/2 signaling pathway-dependent upregulation of Beclin1. Oncol Lett, 2016;11(2): 1051-1056.
21. Peng, X, et al. Apelin-13 induces MCF-7 cell proliferation and invasion via phosphorylation of ERK1/2. Int J Mol Med, 2015;36(3): 733-8.
22. Salman, T, et al. Serum apelin levels and body composition changes in breast cancer patients treated with an aromatase inhibitor. J BUON, 2016;21(6): 1419-1424.
23. Ahmed, S.A, R.M. Gogal, Jr, J.E. Walsh, A new rapid and simple non-radioactive assay to monitor and determine the proliferation of lymphocytes: an alternative to [3H]thymidine incorporation assay. J Immunol Methods, 1994;170(2): 211-24.
24. Nociari, M.M, et al. A novel one-step, highly sensitive fluorometric assay to evaluate cell-mediated cytotoxicity. J Immunol Methods, 1998;213(2): 157-67.
25. Goegan, P, G. Johnson, R. Vincent, Effects of serum protein and colloid on the alamarBlue assay in cell cultures. Toxicol In Vitro, 1995;9(3): 257-66.
26. Available from: (https://www.proteinatlas.org/ENSG00000134817-APLNR/tissue). .
27. Bai, B, et al. Heterodimerization of apelin receptor and neurotensin receptor 1 induces phosphorylation of ERK(1/2) and cell proliferation via Galphaq-mediated mechanism. J Cell Mol Med, 2014;18(10): 2071-81.
28. Wang, K, et al. Synergistic anti-breast cancer effect of pulsatilla saponin D and camptothecin through interrupting autophagic-lysosomal function and promoting p62-mediated ubiquitinated protein aggregation. Carcinogenesis, 2019.
29. Villanueva-Paz, M, et al. AMPK Regulation of Cell Growth, Apoptosis, Autophagy, and Bioenergetics. Exp Suppl, 2016;107: 45-71.
30. Choi, J, Y.J. Cha, J.S. Koo, Adipocyte biology in breast cancer: From silent bystander to active facilitator. Prog Lipid Res, 2018;69: 11-20.
31. Blanquer-Rossello, M.M, et al. Leptin Modulates Mitochondrial Function, Dynamics and Biogenesis in MCF-7 Cells. J Cell Biochem, 2015;116(9): 2039-48.
32. Huang, H.L, et al. Trypsin-induced proteome alteration during cell subculture in mammalian cells. J Biomed Sci, 2010;17: 36.
33. Calebiro, D. A. Godbole, Internalization of G-protein-coupled receptors: Implication in receptor function, physiology and diseases. Best Pract Res Clin Endocrinol Metab, 2018;32(2): 83-91.
34. Cottrell, G.S, Roles of proteolysis in regulation of GPCR function. Br J Pharmacol, 2013;168(3): 576-90.
35. Aakvaag, A, et al. Growth control of human mammary cancer cells (MCF-7 cells) in culture: effect of estradiol and growth factors in serum-containing medium. Cancer Res, 1990;50(24): 7806-10.
36. Wang, Z, G.H. Greeley, Jr, S. Qiu, Immunohistochemical localization of apelin in human normal breast and breast carcinoma. J Mol Histol, 2008;39(1): 121-4.
37. Li, Y, Y. Chen, AMPK and Autophagy. Adv Exp Med Biol, 2019;1206: 85-108.
38. Krieg, S, et al. Studying the Role of AMPK in Autophagy. Methods Mol Biol, 2018;1732: 373-391.
39. El-Masry, O.S, B.L. Brown, P.R. Dobson, Effects of activation of AMPK on human breast cancer cell lines with different genetic backgrounds. Oncol Lett, 2012;3(1): 224-228.
40. Taliaferro-Smith, L, et al. LKB1 is required for adiponectin-mediated modulation of AMPK-S6K axis and inhibition of migration and invasion of breast cancer cells. 2009;28(29): 2621-33.
41. Wu, Y, et al. Combined inhibition of glycolysis and AMPK induces synergistic breast cancer cell killing. Breast Cancer Res Treat, 2015;151(3): 529-39.
42. Lee, J.O, et al. Rhus verniciflua extract modulates survival of MCF-7 breast cancer cells through the modulation of AMPK-pathway. Biol Pharm Bull, 2014;37(5): 794-801.
43. Lee, Y.K, O.J. Park, Regulation of mutual inhibitory activities between AMPK and Akt with quercetin in MCF-7 breast cancer cells. Oncol Rep, 2010;24(6): 1493-7.
44. Zhang, K, Y. Li, Effects of ginsenoside compound K combined with cisplatin on the proliferation, apoptosis and epithelial mesenchymal transition in MCF-7 cells of human breast cancer. Pharm Biol, 2016;54(4): 561-8.
45. Queiroz, E.A, et al. Metformin induces apoptosis and cell cycle arrest mediated by oxidative stress, AMPK and FOXO3a in MCF-7 breast cancer cells. PLoS One, 2014;9(5): e98207.
46. Fodor, T, et al. Combined Treatment of MCF-7 Cells with AICAR and Methotrexate, Arrests Cell Cycle and Reverses Warburg Metabolism through AMP-Activated Protein Kinase (AMPK) and FOXO1. PLoS One, 2016;11(2): e0150232.
47. Kim, M.Y, et al. Induction of Apoptosis by Citrus unshiu Peel in Human Breast Cancer MCF-7 Cells: Involvement of ROS-Dependent Activation of AMPK. Biol Pharm Bull, 2018;41(5): 713-721.
48. Yue, P, et al. Apelin decreases lipolysis via G(q), G(i), and AMPK-Dependent Mechanisms. Endocrinology, 2011;152(1): 59-68.
49. Yang, X, et al. Apelin-13 stimulates angiogenesis by promoting crosstalk between AMP-activated protein kinase and Akt signaling in myocardial microvascular endothelial cells. Mol Med Rep, 2014;9(5): 1590-6.
50. Bao, H.J, et al. Apelin-13 as a novel target for intervention in secondary injury after traumatic brain injury. Neural Regen Res, 2016;11(7): 1128-33.
51. Huang, J, et al. Apelin protects against liver X receptor-mediated

steatosis through AMPK and PPARalpha in human and mouse hepatocytes. Cell Signal, 2017;39: 84-94.

52. Hou, J, et al. Apelin promotes mesenchymal stem cells survival and vascularization under hypoxic-ischemic condition in vitro involving the upregulation of vascular endothelial growth factor. Exp Mol Pathol, 2017;102(2): 203-209.
53. Stockebrand, M, et al. Differential regulation of AMPK activation in leptin- and creatine-deficient mice. FASEB J, 2013;27(10): 4147-56.
54. Harford-Wright, E, et al. Pharmacological targeting of apelin impairs glioblastoma growth. Brain, 2017;140(11): 2939-2954.